Particle image velocimetry study of a cloud-like flow

L. Venkatakrishnan[†,]*, R. Elavarasan[#], G. S. Bhat[‡], A. Krothapalli and L. Lourenco****

[†]Experimental Aerodynamics Division, National Aerospace Laboratories, Bangalore 560 017, India
[#]Resonetics Inc., 4 Bvd. Way, Building 21, Nashua, NH, USA
[‡]Centre for Atmospheric and Oceanic Sciences, Indian Institute of Science, Bangalore 560 012, India
**Department of Mechanical Engineering, Fluid Mechanics Research Laboratory, Florida A&M University and Florida State University, Tallahassee, FL 32310, USA

This study employs particle image velocimetry (PIV) on a jet with and without subjection to internal heating. The effects of buoyancy enhancement on the entrainment coefficient and on the streamline structures responsible for it are investigated. PIV results for the unheated jet are in good agreement with earlier studies. It is shown that when internal heating is present in the flow, the mean entrainment coefficient decreases from a value of 0.057 characterizing a standard jet to 0.017, at a heating rate of 1400 W corresponding to a Richardson number of 0.24. It is also shown that the mingling of the entrained fluid with the main flow is different in heated and unheated jets.

IT has been recognized since long that cumulus clouds get diluted due to the ambient air entering them[1]. This process, known as entrainment, affects cloud development, amount of precipitation and the response of the large-scale atmosphere to cloud convection[2,3]. Majority of the cloud models are based on the plume analogy in which the entrainment from the lateral side is continuous and the entrained fluid mixes across the flow instantaneously[4]. The plume model employs an entrainment relationship of the type conceived first by Taylor (ref. 5), which postulates that the mean inflow velocity across the edge (V_e) of a free turbulent shear flow is proportional to a characteristic velocity within the flow, usually taken as the local time-averaged maximum mean velocity along the axis of the flow (U_c). Taylor's hypothesis has been successful in a variety of situations (ref. 6), but when applied to clouds it has failed to make realistic predictions of either liquid water concentrations or height of penetration[7,8]. Later studies based on *in situ* observed thermodynamic properties showed that some (but not all) air from cloud base rises to high levels within growing clouds, without being diluted by entrainment[9,10]. Thus, while there is no doubt that clouds do get diluted due to entrainment, the mechanism seems to be different from that implied by Taylor's hypothesis. There have been attempts directed towards predicting the amount of entrainment into cumulus clouds using alternate models (reviewed in refs 11 and 12); however their scientific basis remains obscure. For example, in the episodic mixing model of Raymond and Blyth[13], a part of the cloud air mixes with ambient air and seeks a new vertical level for settling where it can mix again, and the process continues. This model, designed to predict the observed cloud properties, works reasonably well in some specific cases, but its applicability is limited because the specification of the amount of ambient air mixing with the cloud air at each level is *ad hoc*.

The difficulty in developing a realistic entrainment model for cumulus clouds lies in the fact that the dynamical consequences of some important physical processes specific to cloud flows are yet to be quantified. Flow inside a cumulus cloud differs from that in ordinary plumes and thermals[6] in that the latent heat released following the condensation of water vapour locally enhances the buoyancy and the flow accelerates (as opposed to $x^{-1/n}$ decay in velocity, where x is the distance from the source and n is a constant not less than 1, e.g. see ref. 6), except for some distance near the cloud top (ref. 14), and the surrounding air is stably stratified. The theoretical progress is constrained by the very nature of the flow inside clouds being highly complex and turbulent, and the governing nonlinear partial differential equations preclude direct numerical solutions. The remote location of clouds, their short lifespan (typically 15–30 min) and highly transient nature of the flow make detailed *in situ* measurements of properties impossible. Though laboratory models are possible, it is not a simple task to reproduce a cumulus cloud in the laboratory in all detail, and only certain specific aspects can be addressed at a time.

Here we focus on the effect of condensational heating in clouds. There have been attempts in the past to investigate flows with increasing buoyancy – on accelerating thermals by Turner[15], on jets by Ricou and Spalding[16], and on free shear flows by Hermanson and Dimotakis[17]. These studies employed chemical reactions for producing increase in buoyancy. The results from these studies are not directly applicable to clouds because buoyancy enhancement was a result of mixing of two chemicals. Thus, the effect on mixing due to enhancement of buoyancy cannot be unambiguously isolated. A series of laboratory experiments carried out at the Centre for

*For correspondence. (e-mail: venkat@ead.cmmacs.ernet.in)

Atmospheric and Oceanic Sciences, Indian Institute of Science (IISc), Bangalore using a volumetric heat injection method more closely simulated condensational heating in clouds[18–20]. Results from the flow visualization studies and laser doppler velocimeter (LDV) measurements revealed drastic changes in the flow structure and entrainment upon local heating[20,21].

Though a plume is a much closer approximation to a cloud[4], the consequences of volumetric heating on jets and plumes are found to be broadly similar[20]. It is easier to produce a jet flow, and more data are available on jets with and without subjection to volumetric heating. Therefore, a jet is chosen for the present study.

The entrainment in the IISc studies was estimated by computing the mass flux by integrating a fit to the measured radial profiles of axial velocity at different axial locations. There are problems in accurately measuring the (very low) velocities at the flow edges using LDV, and this introduces some uncertainty in the estimated mass flux. Further, the transient nature of the experiment required measurements at different axial locations to be carried out on different days, thus demanding a high degree of reproducibility. In order to overcome these issues, the particle image velocimetry (PIV) technique was employed in the present study. PIV enables a study of the instantaneous flow field in addition to the time-averaged values. Using the entrainment velocity (defined later) obtained from the averaged flow field, we attempt a more direct estimation of the entrainment coefficient than through computation of the mass flux.

Experimental set-up

The experiments were carried out in a water tank. A schematic of the experimental arrangement and the flow configuration are shown in Figure 1. The tank size is chosen based on the requirement for the jet to effectively discharge into an infinite environment to reduce the effects of confinement and ensure conservation of momentum, as suggested by Hussein *et al.*[22]. The jet is fed from a constant-head tank whose height can be varied to

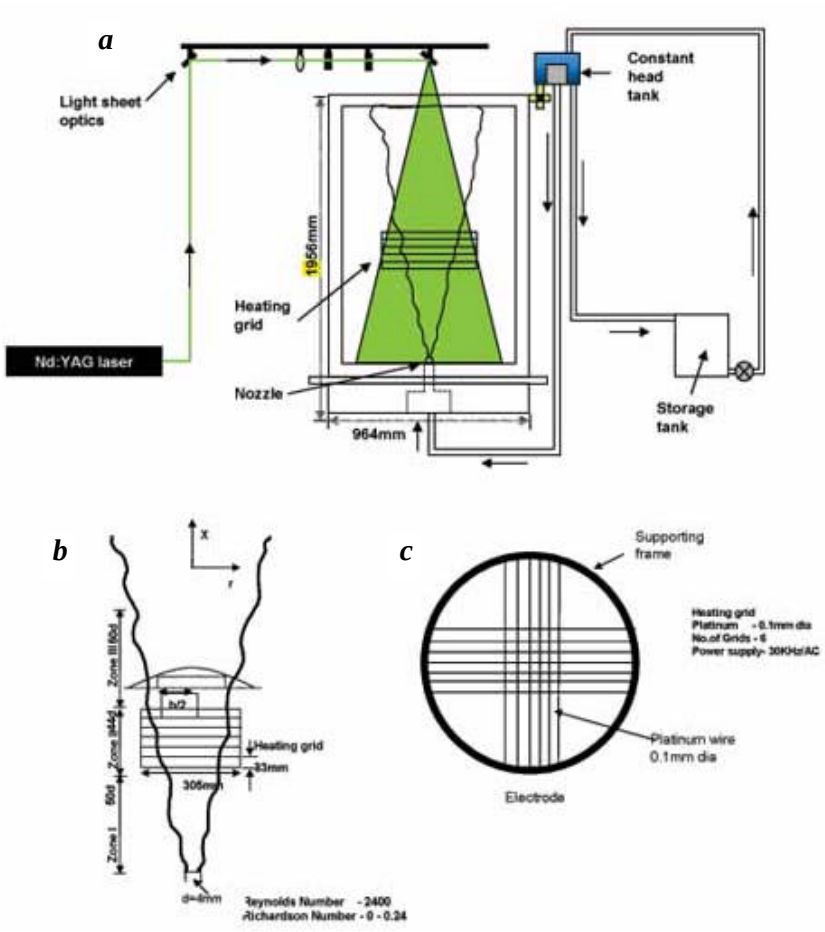

Figure 1. ***a***, Schematic of experimental arrangement; ***b***, Flow geometry, and ***c***, Electrode.

obtain different flow rates. The exit momentum flux is constant to within ± 1% over the duration of the experiment, as inferred from measurements of velocity at the nozzle exit. The diameter d of the nozzle from which the jet issues is 4 mm and the exit velocity is 0.61 m s^{-1}. This gives a Reynolds number of 2440 based on exit velocity and diameter.

The enhancement of buoyancy is achieved by the volumetric heat injection method developed by Bhat *et al.*[23]. The heat is injected into the flow by placing suitable electrodes (Figure 1 *c*) and applying high-frequency alternating voltage between them. The electrodes were made of fine platinum wires (100 μm) netted on a thin circular supporting frame, placed horizontally across the flow at desired heights. The effect of the wires on the flow is negligible as the Reynolds number based on wire diameter is less than 5. A high-frequency (30 kHz) alternating voltage is applied between the electrodes. Varying the voltage across the electrodes controlled the amount of heat input to the jet. Heat was added over the region from 50d to 94d from the nozzle exit. This choice of location of the heat-injection zone ensures that the flow has the properties of a fully developed jet before being subjected to volumetric heating. For the sake of simplicity, the jet with and without off-source heat injection will be referred to from hereupon as the 'heated jet' and 'unheated jet', respectively; the pre-heat-injection zone will be referred to as zone I, the heat-injection zone as zone II and the post-heat-injection zone as zone III.

The tank is filled with filtered and de-ionized water to ensure a non-conducting ambient fluid. To ensure that only the jet fluid is rendered electrically conductive, a small amount of HCl (~ 4 ml/l of water) is added to the jet fluid. Adding an appropriate amount of acetone neutralizes the increase in buoyancy of the jet fluid due to the addition of HCl. Since ions from the ambient fluid have been removed, only the fluid that has mixed with the original jet fluid conducts electricity and gets volumetrically heated. It can be shown that the heat release rate in the jet is directly proportional to the acid concentration[21]. The Clausius–Clapeyron relation for saturation vapour pressure implies that the latent heat release in clouds is proportional to the saturation water vapour mixing ratio in clouds (see ref. 14, pp. 57–59). Thus, the acid concentration in the jet is a proxy for the water vapour in the clouds, making the present technique more relevant to clouds compared to those based on chemical reactions.

The PIV technique is based on the concept of measuring displacement of the particles seeded in the flow. Two consecutive images of the seeding particles are recorded within a short time interval (Δt). By measuring the particle displacement in the image in time Δt, the velocity in the flow field is calculated. Details of the present PIV data processing scheme can be found in Lourenco and Krothapalli[24], and the procedure is briefly described here. A double-pulsed, digitally sequenced Nd : YAG laser (Spectra-Physics, 400 mJ) was used. A light sheet of one mm thickness was created by suitable combination of spherical and cylindrical lenses. The images were recorded using a cross-correlation CCD camera (Kodak ES1.0) whose axis was perpendicular to the flow axis. The resolution of the camera is 1 k × 1 k and is operated in double-pulsed mode. In this mode of operation, with proper synchronization with laser pulses, the camera can acquire double images at a rate of 15 image pairs per second. The imaging area is 150 mm × 150 mm square section (1 pixel ~ 0.18 mm). The time between pulses was optimized between 8 and 35 ms depending on the location of the flow (lower near the nozzle exit and higher in zone III). The double-pulsed images were acquired through an Imaging Technologies ICPCI frame-grabber board, which resides on a single slot of the PCI bus of a personal computer.

Three examples of double-exposed particle images are shown in Figure 2. The particle density is maintained sufficiently large to enable the computation of velocity field at high spatial resolutions. Though we see some structures in the images, it is difficult for the eye to make out the velocity field, but not so for a computer using a sophisticated PIV algorithm. The doubly-exposed particle image is divided into many interrogation cells and by performing the cross-correlation on the particle images, the displacement between the particles can be accurately measured and the velocity (displacement) vector assigned at the mid-distance between particle images pairs. Therefore each particle pair contributes to a second-order

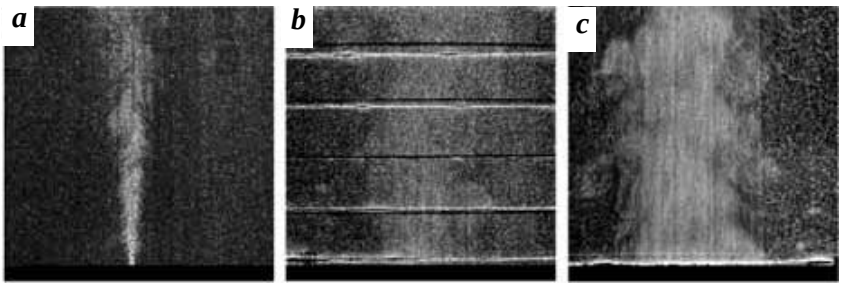

Figure 2. Typical double-exposed particle images in ***a***, Zone I; ***b***, Zone II, and ***c***, Zone III.

approximation of the velocity. However, in contrast to the traditional approach which uses structured grids, these velocities are evaluated in an unstructured grid. The flow field at any point is described by an analytical function using a least squares fitting algorithm. The function that is used is a second-order polynomial,

$$\vec{u} = \vec{a}x^2 + \vec{b}x + \vec{c}y^2 + \vec{d}y + \vec{e}xy + \vec{f}. \quad (1)$$

The marked advantage of this approach is that the flow field is described at every point with second-order accuracy, including the derivatives that are found by differentiating the above equation. The error minimization approach maintains the order of the accuracy and provides a means for accurate evaluation of the field derivatives. It has been demonstrated[24] that this approach provides substantial improvement in accuracy and spatial resolution over traditional PIV methods.

The size of each interrogation cell used here is 8×8 pixels, yielding a total of 15,625 vectors per image. For each case described in the present article, 250 instantaneous double-exposed images were collected. This corresponds to measurement duration of about 17 s – the time limit set by the capability of the data-acquisition system. The number of images collected, while reasonable for the mean velocity field (large eddy turnover time approximately 1.5 s), is unsatisfactory for turbulent velocity measurements and hence only mean velocity measurements are presented here.

Results and discussion

Both instantaneous and mean velocity and vorticity fields were measured for three different heating rates. A non-dimensional number based on inertia and buoyancy forces, namely a Richardson number defined as

$$\mathrm{Ri} = \frac{ag}{rC}\frac{1}{b_b}\frac{Q}{U_b^3}, \quad (2)$$

seems to govern the flow behaviour[18]. In eq. (2), a is the coefficient of thermal expansion, C is the specific heat of water and b_b and U_b are respectively, the length and velocity scales at the entry to the heat injection zone (see Figure 1 *b*). The length scale is taken as the radial distance at which the axial velocity falls to $1/e$ times its centreline value (denoted by b_u) and the velocity scale is the local centreline velocity of the jet.

Table 1 shows representative values of some flow parameters for cumulus and cumulonimbus clouds, and the flow generated for the present study. The cloud widths shown here are the radii of the clouds and the vertical velocity corresponds to that observed at lower levels in clouds (e.g., see ref. 14, pp. 158–166; ref. 25). Further, a typical cloud temperature excess of 0.2 to 1°C over the environment is assumed. The larger cloud is assumed to have more buoyancy. It is seen from Table 1 that Ri ranges from 0.2 to 2 for cumulus and from 0.3 to 3 for cumulonimbus clouds. Hence the present experiments, in which Ri assumes values of 0.068, 0.12 and 0.24 for heat inputs of 400, 700 and 1400 W respectively, may be considered to have close dynamical similarity with the lower range of cumulus clouds as far as buoyancy effects are concerned.

PIV measurements were carried out separately for each zone. As can be seen in Figure 2 *b*, the shadows of the grid and the wire mesh cause a non-uniform illumination in zone II resulting in discontinuous regions of velocity data and hence vorticity between the grids – a problem being currently addressed. Hence vorticity results for zone II are not presented. The study by Elavarasan *et al.*[18] has shown that the effect of heating on the jet growth is mainly in the later part of zone II and the earlier part of zone III. Therefore, important changes are captured by studying zone III itself.

The variation of the axial component of centreline velocity U_{cl} along the jet axis is shown in Figure 3. For the unheated jet, U_{cl} is expected to vary as x^{-1} (ref. 6). While this is strictly not so for the entire range of x/d shown, over smaller x/d ranges, namely 100–140 and 140–180, x^{-1} variation is seen. (The x/d range covered in one set of PIV measurements is about 40, and the discontinuity in slope is perhaps due to changed flow conditions between experiments.) The scatter in the data indicates that the averaging time ($\sim$ 17 s) is not sufficient to get steady-state velocity values. Nevertheless, the effect of heating on the decay rate of U_{cl} is clearly brought out in Figure 3. In particular, at 1400 W heating rate, U_{cl} shows little variation with x in zone III. It may be recalled here that in the case of plume (which is a purely buoyancy-driven flow, a jet is momentum-driven and in the heated jet, both buoyancy and momentum are important), U_{cl} decreases as $x^{-1/3}$ (ref. 6). The near constant value of U_{cl} in zone III for the heated jet at 1400 W heating rate reveals that the locally heated jet is neither jet-like nor plume-like, and very different.

Table 1. Estimation of Ri for clouds and for the present flow

Flow	Width B (m)	Velocity U (m/s)	$(\Delta r/r) \times 10^3$	Ri
Cumulus*	250–500	2–4	0.5–1.7	0.1–2
Cumulonimbus*	500–2000	2–5	1.7–3.5	0.3–3
Jet	24×10^{-3}	50×10^{-3}	0.7–2.6	
d = 4 mm, z/d = 50				
Q = 400 W				0.068
Q = 700 W				0.12
Q = 1400 W				0.24

*See text for details.

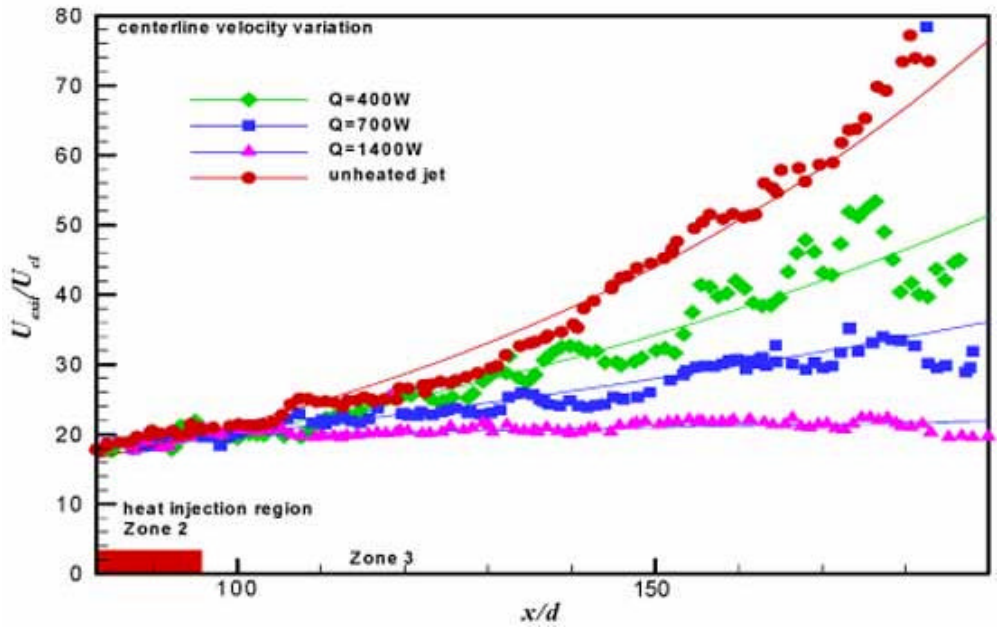

Figure 3. Effect of different heating rates on the centreline velocity decay in zone III.

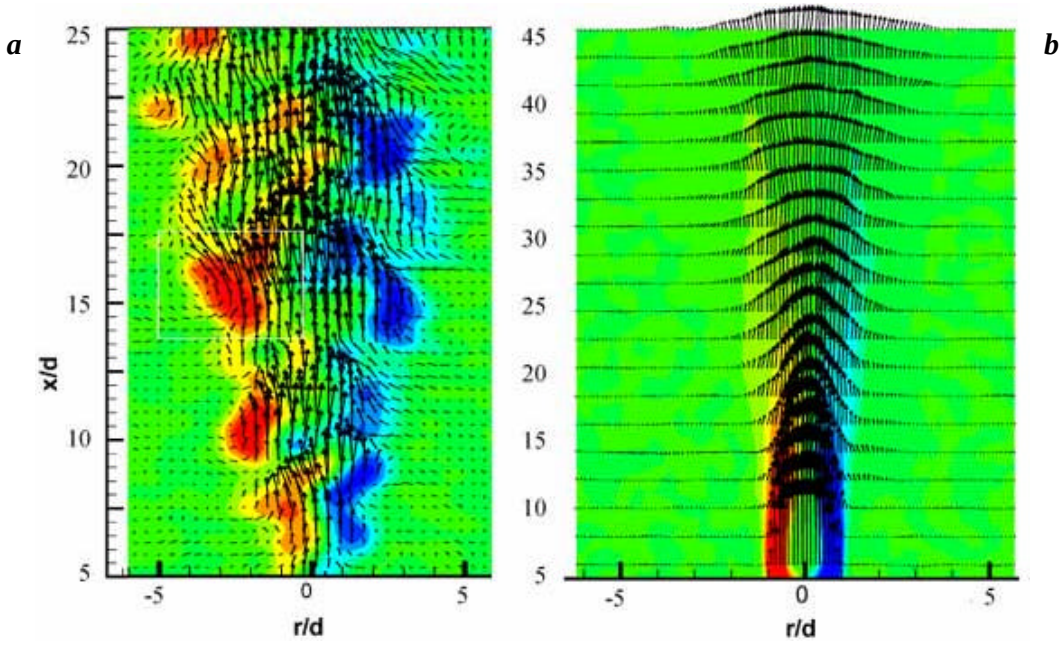

Figure 4. Velocity and vorticity field of the jet in zone I. ***a***, Instantaneous field, and ***b***, Averaged field.

Figure 4 shows typical vorticity and velocity fields in the plane of observation from the PIV measurements in zone I. The vector length represents the magnitude of the velocity at that location and the contours show the magnitude of the out of plane component of vorticity. The red and blue regions correspond to those of positive and negative vorticity respectively. Figure 4 *a*, which is an instantaneous flow field of the jet, shows regions of concentrated vorticities on either side of the jet axis. It is observed that the horizontal component of velocity is significantly enhanced in the outer parts of the jet associated with these vortices. These represent the coherent

structures in the flow which are mainly responsible for the entrainment of the ambient fluid. Radial inflow of fluid towards the jet axis (i.e. entrainment) is clearly seen in Figure 4 *a*. However, even near the lateral sides of the frame which are away from the centres of strong vorticity, the instantaneous horizontal inflow velocities are not smoothly varying functions of *x*, but seem to be influenced by the coherent structures in the jet. Figure 4 *b* shows the mean flow field and the development of the jet. The axial component of velocity has a top hat profile at the nozzle exit and is transformed into a Gaussian-looking profile beyond 15*d* from the exit. The lateral spread of the jet and axial decay of mean velocity and vorticity are clearly seen.

Figures 5 and 6 show the instantaneous and average streamline patterns and vorticity contours in unheated and heated jets, respectively. The streamline pattern is distinctly different between heated and unheated jets. In the unheated jet, undulations in the streamlines that seem to be drawn into the flow in a circular kind of motion, especially in the outer part of the flow are seen. In the heated jet, streamlines are straight and almost vertical

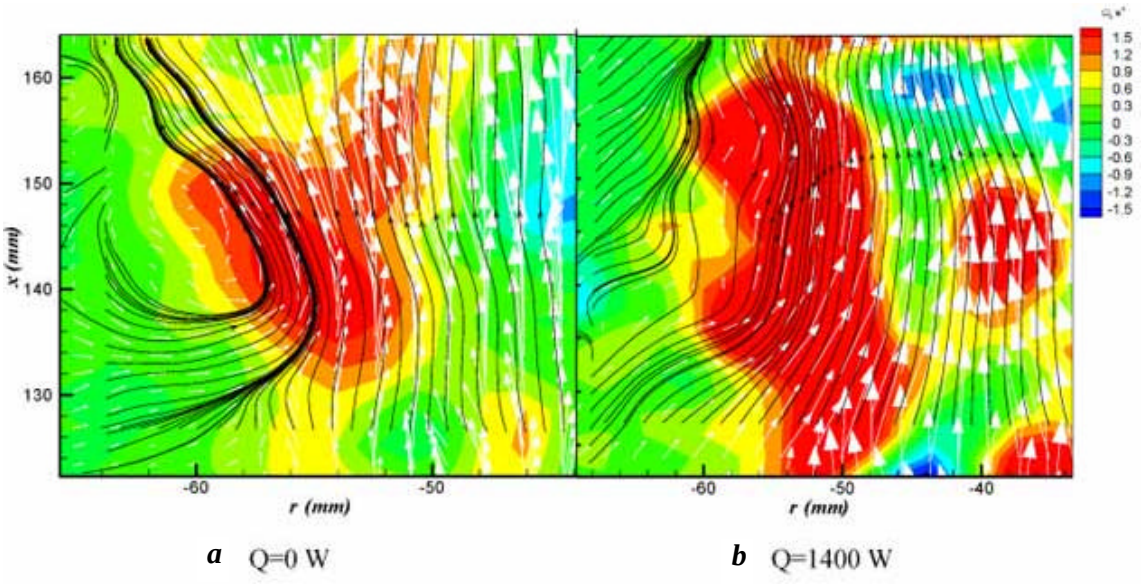

Figure 5. Close-up view of a large-scale structure. ***a***, Unheated jet, and ***b***, Heated jet.

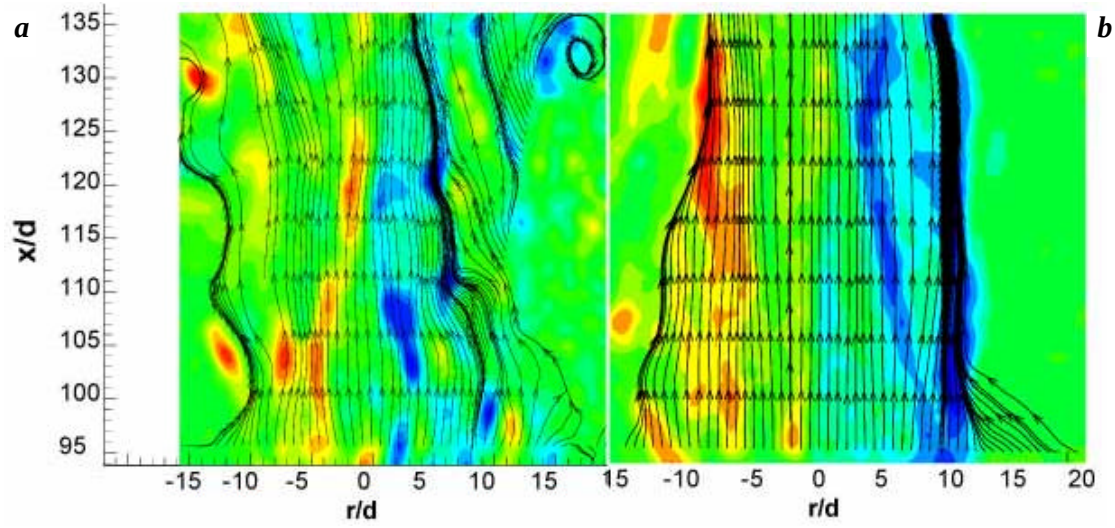

Figure 6. Streamtrace of the entrainment field of (***a***) unheated and (***b***) heated (Q = 1400 W) jet in zone III.

around the jet axis (Figure 6). The vortical structures that characterize the unheated jet are lacking in the heated jet, and the engulfed fluid tends to move up along the edges of the flow. Dye-flow visualization pictures had suggested a change in the large eddy structure of the jet upon heating[21], and this has been clearly brought out in Figure 6.

As we have seen in Figure 4, the velocity rapidly decays in the horizontal direction; however, even at large radial distances, velocity is not identically equal to zero, i.e. there is no well-defined boundary in the flow. For the purpose of defining the entrainment velocity, the edge of the jet is defined as the radial distance over which the axial velocity has fallen to $1/e$ of its centreline value, and the radial (horizontal) component of velocity at this point is taken to be the entrainment velocity, V_e (ref. 6). More specifically,

$$V_e = \alpha U_c, \tag{3}$$

where α is called the entrainment coefficient. From the continuity of mass, it can be shown that the mass flux m and V_e are related by

$$\frac{dm}{dx} = 2\pi b_u V_e. \tag{4}$$

Using measured values of U_c, V_e and eq. (2), α has been calculated in zone III, and the results are shown in Figure 7. The case of Ri = 0.24 is chosen to show the maximum of the effect. Values of α are not constant but vary with x, despite the fact that axisymmetry over the averaging period has not been assumed (i.e. the values of U_c and V_e used in eqs (3) and (4) are obtained from the corresponding axial sections of the flow). This variation is mainly due to the relatively short averaging time used here (not long enough to remove the contribution of individual large vortical structures). Also, and we expect α to be independent of x in the unheated case, if sufficiently long time averages are taken. The average value of α for the axial range covered (shown by the dotted lines in Figure 7) is 0.057 for the unheated case. This is close to the value of 0.056 suggested by Turner[6] for a jet based on conventional measurements. For the heated case, the average value of α is 0.017, i.e. only 30% of the unheated value. Thus, there is a large reduction in the entrainment coefficient.

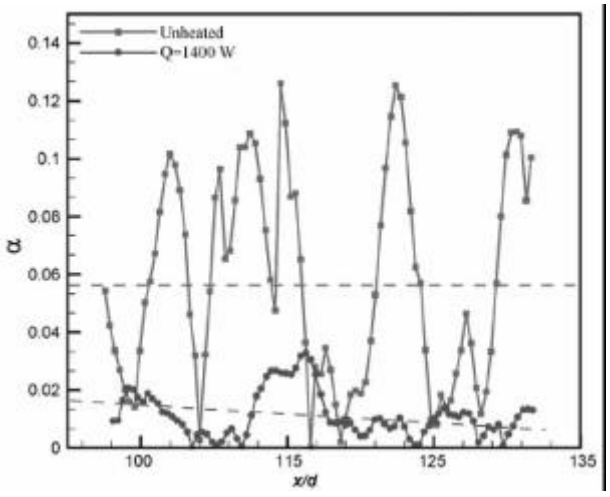

Figure 7. Variation of entrainment coefficient with axial distance in zone III.

Discussion and conclusion

The present measurements provide direct evidence that the entrainment constant α reduces drastically in the inner region of the jet, thus reducing the incursion of the ambient fluid to the core of the flow when volumetric heating is applied. Figures 5 and 6 reveal that when viewed as a whole, there is a net inflow of mass towards the jet axis in both unheated and heated cases. However, this fluid is confined to the outer parts of the flow in the heated jet, enabling the fluid in the jet axial region to move up undiluted. Thus there is entrainment, but mixing does not spread across the flow, similar to what had been observed in cumulus clouds based on aircraft observations. These results also provide support to the scenario suggested by Bhat and Narasimha[21] for cumulus clouds, that the disruption of the coherent structures caused by the latent heat release results in fluid rising practically undiluted in the central core, and entrainment of ambient fluid and mixing remain confined to the cloud edges.

The present study has shown that PIV is a very powerful and convenient measurement tool in the study of cloud-like flows. While the phenomenon of volumetric heating disrupting the large eddies and reducing entrainment had been observed by previous efforts, measurement of the vorticity fields and estimation of the entrainment coefficient is made possible using PIV. The results are certainly encouraging and further work needs to be carried out. The value of the Richardson number in the present experiments at the largest heating rate applied (Ri = 0.24) lies near the lower range for cumulus clouds in the atmosphere (Table 1). The averaging time duration can be extended to obtain the variation of α as a function of axial distance from the start of the heat-injection zone. Further, the shadows of the wire grids in zone II prevented a study of the changing vorticity field – addressing this would enable a check on whether there is a predominant kind of vorticity after heating. If these are accomplished, then we obtain a detailed picture of the axial variation of α with Ri that may be applied in the formulation of a better cumulus cloud model with inputs from the already available *in situ* measurements on clouds.

1. Stommel, H., *J. Meteorol.*, 1947, **49**, 1334–1347.
2. Arakawa, A. and Schubert, W. H., *J. Atmos. Sci.*, 1974, **31**, 674–701.
3. Lord, S. J. and Arakawa, A., *J. Atmos. Sci*., 1980, **37**, 2677–2692.
4. Emanuel, K. A., *Atmospheric Convection*, Cambridge University Press, 1994.
5. Morton, B. R., Taylor, G. I. and Turner, J. S., *Proc. R. Soc. London, Ser A*, 1956, **234**, 1–23.
6. Turner, J. S. *J. Fluid Mech.*, 1986, **173**, 431–471.
7. Squires, P. and Turner, J. S., *Tellus*, 1962, **14**, 422–434.
8. Warner, J., *J. Atmos. Sci.*, 1970, **27**, 1035–1040.
9. Paluch, I. R., *J. Atmos. Sci.*, 1979, **36**, 2467–2478.
10. LaMontagne, R. G. and Telford, J. W., *J. Atmos. Sci.*, 1983, **40**, 2148–2156.
11. Reuter, G. W., *Bull. Am. Meteorol. Soc.*, 1986, **67**, 151–154.
12. Blyth, A. M., *J. Appl. Meteorol.*, 1993, **32**, 626–641.
13. Raymond, D. J. and Blyth, A. M., *J. Atmos. Sci.*, 1986, **43**, 2708–2718.
14. Ludlam, F. H., *Clouds and Storms*, Pennsylvania University Press, 1980, p. 166.
15. Turner, J. S., *Q. J. R. Meteorol. Soc*., 1963, **89**, 62–74.
16. Ricou, F. P. and Spalding, D. B., *J. Fluid Mech.*, 1961, **11**, 21–23.
17. Hermanson, J. C. and Dimotakis, D. E., *J. Fluid Mech*., 1989, **199**, 333–375.
18. Elavarasan, R., Bhat, G. S., Prabhu, A. and Narasimha, R., *Fluid Dyn. Res.*, 1995, **16**, 189–202.
19. Venkatakrishnan, L., Bhat, G. S., Prabhu, A. and Narasimha, R., *Curr. Sci*., 1998, **74**, 597–606.
20. Venkatakrishnan, L., Bhat, G. S., Prabhu, A. and Narasimha, R., *J. Geophys. Res*., 1999, **104**, 14271–14281.
21. Bhat, G. S. and Narasimha, R., *J. Fluid Mech*., 1996, **325**, 303–330.
22. Hussein, J. H., Capp, S. P. and George, H. K., *J. Fluid Mech.*, 1994, **258**, 31–75.
23. Bhat, G. S., Narasimha, R. and Arakeri, V. H., *Exp. Fluids*, 1989, **7**, 99–102.
24. Lourenco, L. and Krothapalli, A., Proceedings of the International Conference on Optical Technology and Image Processing in Fluid, Thermal and Combustion Flows, Yokohama, 1998.
25. LeMone, M. A. and Zipser, E., *J. Atmos. Sci*., 1980, **37**, 2444–2457.

Received 22 April 2003; revised accepted 25 June 2003